Enhanced global mathematical model for studying cerebral venous blood flow

L. O. Müller & E. F. Toro
Laboratory of Applied Mathematics
University of Trento
Via Mesiano 77, 38123 Trento, Italy
e-mail: lucas.mueller@ing.unitn.it, toro@ing.unitn.it

Isaac Newton Institute for Mathematical Sciences. University of Cambridge, UK. April, 2014.

15 April 2014

Enhanced global mathematical model for studying cerebral venous blood flow

L. O. Müller & E. F. Toro

Laboratory of Applied Mathematics
University of Trento
Via Mesiano 77, 38123 Trento, Italy
e-mail: lucas.mueller@gmail.com, toro@ing.unitn.it

15 April 2014

Abstract

Here we extend the global, closed-loop, mathematical model for the cardiovascular system in [18] to account for fundamental mechanisms affecting cerebral venous haemodynamics: the interaction between intracranial pressure and cerebral vasculature and the Starling-resistor like behaviour of intracranial veins; an updated version of a valve model is also included. Computational results are compared with MRI-derived flow measurements and cerebral venous flow waveforms are discussed in light of current physiological concepts and model-driven considerations.

1 Introduction

Recent developments on the potential link between extracranial venous anomalies and neurological conditions have increased interest on the physiology of cerebral venous return, currently, a poorly understood subject [23]. A prominent example is Chronic CerebroSpinal Venous Insufficiency (CCSVI) and its potential link to Multiple Sclerosis (MS) [31]. Interest in this area has been further increased by very recent findings on altered cerebrospinal fluid dynamics in MS patients [16] and by reported improvements of such dynamics, as well the clinical course of the disease, after treatment of MS/CCSVI patients with percutaneous transluminal angioplasty (PTA) [32].

In this paper we are concerned with the development of a mathematical model to study cerebral haemodynamics. To this end we construct an extension of the closed-loop model for the cardiovascular system reported in [18] to account for two relevant factors. First we deal with the interaction of the cerebral vasculature with the pulsating intracranial pressure, for which we adopt the model proposed in [26, 27]; this model describes the variation of intracranial pressure in time in terms of the variation of cerebral blood volume. Second, we incorporate a model to account for the Starling-resistor like behaviour of cerebral veins. This is supported by experimental evidence that shows that pressure in cerebral veins is always higher than intracranial pressure, for a wide range of intracranial pressures, independently of the pressure in downstream vessels,

such as the dural sinuses [10, 15]. The underlying mechanism is still the subject of debate, with some researchers speaking in favour of a purely hydraulic mechanism [1] and others hypothesizing a control mechanism [6]. Moreover, there is evidence of distinct morphological and mechanical properties of the terminal portion of cerebral veins, in the vicinity of dural sinuses [29, 5, 6, 3]. In order to model this behaviour, we have added cerebral veins to the venous network in [18] and implemented a simple model for Starling-resistor elements, proposed in [19]. These elements are placed in the vicinity of the point where cerebral veins drain into the dural sinuses. Our model is partially validated by comparing our computational results with MRI-derived flow measurements, obtaining satisfactory agreement. Computational results are discussed in light of current knowledge of the physiology of cerebral venous haemodynamics. The proposed mathematical model constitutes a computational tool suitable for the study of pathologies related to extracranial venous anomalies and their interaction with intracranial haemodynamics. This will be the subject of future investigations.

The rest of the paper is structured as follows. Section 2 describes the extensions made to the model reported in [18]. Section 3 contains computational results and comparison with MRI-derived measurements. Discussion of computational results is found in section 4. Section 5 includes a summary and conclusions.

2 Methods

The model presented in this paper is an extension of the closed-loop model for the cardiovascular system presented in [18], to which the reader is referred to for further details.

2.1 Mathematical model of the cardiovascular system

Our mathematical model includes a one-dimensional description of the networks of major arteries and veins, and lumped-parameter models for the heart, the pulmonary circulation and capillary beds linking arteries and veins, see Fig. 1. Geometrical information for major head and neck veins is obtained from segmentation of MRI data. This patient-specific characterization allows us to compare computational results *versus* patient-specific MRI-derived flow quantification data, see [18].

One-dimensional blood flow in elastic vessels is described by the following system of non-linear, first-order hyperbolic equations

$$\begin{cases} \partial_t A + \partial_x q = 0\,, \\ \partial_t q + \partial_x \left(\hat{\alpha} \dfrac{q^2}{A} \right) + \dfrac{A}{\rho} \partial_x p = -f\,. \end{cases} \tag{1}$$

Here x is the axial coordinate of the vessel; t is time; $A(x,t)$ is cross-sectional area of the vessel; $q(x,t)$ is flow rate; $p(x,t)$ is average internal pressure over a cross-section; $f(x,t)$ is friction force per unit length of the tube; ρ is fluid density and $\hat{\alpha}$ is a coefficient related to the assumed velocity profile. In what follows we assume $\rho = \mathit{constant}$ and $\hat{\alpha} = 1$ (blunt velocity profile). To close the system we adopt a tube law relating $p(x,t)$ to $A(x,t)$ and other parameters,

namely

$$p(x,t) = p_e(x,t) + K(x)\left[\left(\frac{A(x,t)}{A_0(x)}\right)^m - \left(\frac{A(x,t)}{A_0(x)}\right)^n\right] + P_0\,. \tag{2}$$

Here $p_e(x,t)$ is the external pressure. $K(x)$, m, n, $A_0(x)$ and P_0 are parameters that account for mechanical and geometrical properties of the vessel. For a discussion on the choice of these parameters for both, arteries and veins, see [18] and references therein. Fig. 1 depicts a schematic representation of the global model. Fig. 2 shows the venous network for the head and neck used here. Cor-

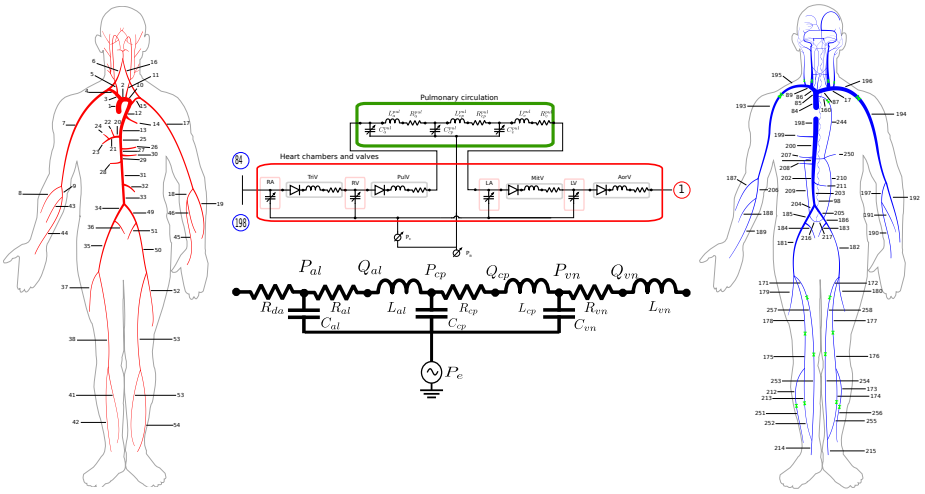

Figure 1: Global, closed-loop model in [18]. Major arteries and veins are modelled one-dimensionally; lumped-parameter models are used for heart, pulmonary circulation, arterioles, capillaries and venules. Left frame: major arteries; middle frame: lumped-parameter models; right frame: major veins.

tical cerebral veins draining into the superior and inferior sagittal sinuses have been added to the venous network in [18]. Note that there is high variability in the number of veins draining into the superior sagittal sinus; our choice is in line with the numbers reported in [29]. Moreover, a Starling-resistor element was added to the end of each cerebral vein (see section 2.3). Table 1 shows geometrical and mechanical properties of vessels added or changed with respect to the venous network of [18]. As a consequence of the venous network extension, the lumped-parameter compartment linking middle and anterior cerebral arteries to the inferior and superior sagittal sinuses has also been modified. The new configuration of this lumped compartment is shown in Fig. 3 and coefficients for lumped elements are found in Table 2.

Table 1: Geometrical and mechanical parameters for veins added, or modified, to the venous network of [18]. L: length; r_0: inlet radius; r_1: outlet radius; c_0: wave speed for $A = A_0$; *Type*: vessel type (1: dural sinus, 9: cerebral vein); Ref : bibliographic source or MRI imaging segmented geometry.

No.	Vessel name	$L\,[cm]$	$r_0\,[cm]$	$r_1\,[cm]$	$c_0\,[m/s]$	Type	Ref.
103	Sup. sagittal sinus	2.50	0.350	0.367	5.000	1	MRI

Table 1 – continued from previous page

No.	Vessel name	$L\,[cm]$	$r_0\,[cm]$	$r_1\,[cm]$	$c_0\,[m/s]$	Type	Ref.
105	Inf. sagittal sinus	3.67	0.160	0.160	5.000	1	MRI
106	Vein of Galen	0.60	0.366	0.400	1.703	9	MRI
149	Sup. sagittal sinus	4.33	0.229	0.258	5.000	1	MRI
150	R. Labbe v.	5.00	0.150	0.150	2.376	9	MRI
151	L. Labbe v.	5.00	0.150	0.150	2.376	9	MRI
152	Sup. sagittal sinus	4.33	0.258	0.287	5.000	1	MRI
153	Sup. sagittal sinus	2.50	0.334	0.350	5.000	1	MRI
157	Sup. sagittal sinus	5.00	0.300	0.334	5.000	1	MRI
158	Cerebral vein	5.00	0.150	0.150	2.376	9	[29]
159	Cerebral vein	5.00	0.150	0.150	2.376	9	[29]
161	Cerebral vein	5.00	0.150	0.150	2.376	9	[29]
162	Cerebral vein	5.00	0.150	0.150	2.376	9	[29]
165	Sup. sagittal sinus	4.33	0.200	0.229	5.000	1	MRI
236	Sup. sagittal sinus	2.00	0.287	0.300	5.000	1	MRI
237	Cerebral vein	5.00	0.150	0.150	2.376	9	[29]
238	Cerebral vein	5.00	0.150	0.150	2.376	9	[29]
239	Cerebral vein	5.00	0.150	0.150	2.376	9	[29]
241	Inf. sagittal sinus	3.67	0.160	0.160	5.000	1	MRI
245	Cerebral vein	3.00	0.150	0.150	2.376	9	[29]
248	Inf. sagittal sinus	3.67	0.160	0.160	5.000	1	MRI
249	Cerebral vein	3.00	0.150	0.150	2.376	9	[29]
260	Cerebral vein	3.00	0.150	0.150	2.376	9	[29]
261	Terminal cerebral vein	1.00	0.150	0.150	5.000	1	[29]
262	Terminal cerebral vein	1.00	0.150	0.150	5.000	1	[29]
263	Terminal cerebral vein	1.00	0.150	0.150	5.000	1	[29]
264	Terminal cerebral vein	1.00	0.150	0.150	5.000	1	[29]
265	Terminal cerebral vein	1.00	0.150	0.150	5.000	1	[29]
266	Terminal cerebral vein	1.00	0.150	0.150	5.000	1	[29]
267	Terminal cerebral vein	1.00	0.150	0.150	5.000	1	[29]
268	Terminal cerebral vein	1.00	0.150	0.150	5.000	1	[29]
269	Terminal cerebral vein	1.00	0.150	0.150	5.000	1	[29]
270	Terminal cerebral vein	1.00	0.150	0.150	5.000	1	[29]
271	Terminal cerebral vein	1.00	0.309	0.366	1.804	9	MRI
272	Terminal cerebral vein	1.00	0.150	0.150	5.000	1	MRI
273	Terminal cerebral vein	1.00	0.150	0.150	5.000	1	MRI

2.2 Intracranial pressure

The cranial cavity is conventionally regarded as a space of fixed volume containing the brain parenchyma, the cerebrospinal fluid (CSF) and the cerebral vasculature. The cranial cavity is then connected to the spinal cavity, which exhibits elastic behaviour, allowing for volume changes. Variations in intracranial blood volume produce fluctuations of intracranial pressure and, consequently, exchange of CSF between the intracranial and spinal subarachnoid spaces. For intracranial pressure p_{ic}, here we adopt the model proposed in [26, 27] given by

$$C_{ic}\frac{dp_{ic}}{dt} = \frac{dV_{cv}}{dt} + \frac{p_c - p_{ic}}{R_f} - \frac{p_{ic} - p_{sss}}{R_0}\,. \tag{3}$$

Here p_c and p_{sss} are capillary and superior sagittal sinus pressures, respectively. V_{cv} is the volume of the cerebral vasculature, given by the sum of the volume occupied by arteries, arterioles, capillaries, venules and veins inside the cranium. C_{ic} is the intracranial compliance, given as

$$C_{ic} = \frac{1}{k_e\, p_{ic}}\,, \tag{4}$$

where k_e is the elastance coefficient of the craniospinal system. Here we use $k_e = 0.15\, ml^{-1}$ [26]. R_f and R_0 are CSF filtration and re-absorption resistances. CSF filtration from the subarachnoid space towards the dural sinuses has been shown to vary linearly with the pressure difference $p_{ic} - p_{sss}$ [7]. CSF outflow resistance is taken as $R_0 = 15\, mmHg\, min\, ml^{-1}$ [7] throughout this paper. Following [26, 27], in order to obtain an average CSF filtration flow rate of $400\,\mu l\, min^{-1}$, R_f is set to $R_f = 48.33\, mmHg\, min\, ml^{-1}$. Note that since physiological cerebral blood flow is approximately $720\, ml\, min^{-1}$, the time

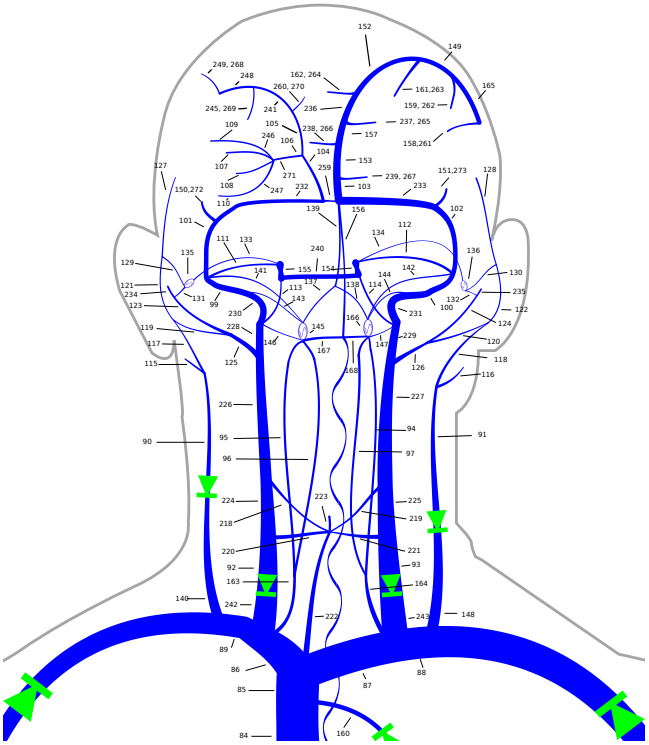

Figure 2: Head and neck veins of the present model. Numbers refer to those used in Table 1, where geometrical and mechanical parameters for each vessel are reported.

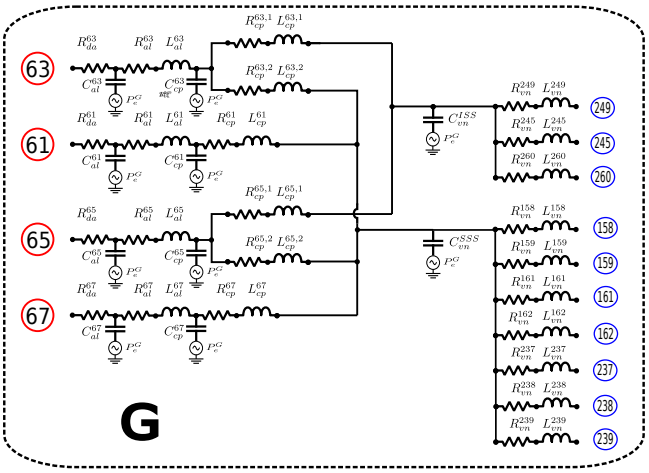

Figure 3: Lumped-parameter compartment **G** resulting from incorporating cortical veins. Numbers on the left refer to feeding arteries, see [18]. Numbers on the right refer to veins draining into sagittal sinuses and are those in Table 1.

Parent/daughter vessel	R_{da}	R_{al}	L_{al}	C_{al}	R_{cp}	L_{cp}	C_{cp}	R_{vn}	L_{vn}	C_{vn}
Lumped model G										
63	20.6859	24.4500	0.0179	0.0070	18.8100	0.0059	0.0007	–	–	–
	–	–	–	–	18.8100	0.0059	–	–	–	–
65	20.6859	24.4500	0.0179	0.0070	18.8100	0.0059	0.0007	–	–	–
61	12.6609	10.5700	0.0078	0.0140	18.8100	0.0059	0.0014	–	–	–
	–	–	–	–	4.0700	0.0013	–	–	–	–
ISS	–	–	–	–	–	–	–	–	–	0.0210
249	–	–	–	–	–	–	–	11.3400	0.0199	–
245	–	–	–	–	–	–	–	11.3400	0.0199	–
260	–	–	–	–	–	–	–	11.3400	0.0199	–
SSS	–	–	–	–	–	–	–	–	–	0.1050
158	–	–	–	–	–	–	–	4.8300	0.0109	–
159	–	–	–	–	–	–	–	4.8300	0.0109	–
161	–	–	–	–	–	–	–	4.8300	0.0109	–
162	–	–	–	–	–	–	–	4.8300	0.0109	–
237	–	–	–	–	–	–	–	4.8300	0.0109	–
238	–	–	–	–	–	–	–	4.8300	0.0109	–
239	–	–	–	–	–	–	–	4.8300	0.0109	–

Table 2: Parameters for artery-vein connection shown in Fig. 3, derived from [13]. R_{da} is resistance for distal arteries, in $mmHg\,s\,ml^{-1}$, R is resistance in $mmHg\,s\,ml^{-1}$, L inductance in $mmHg\,s^2\,ml^{-1}$ and C capacitance in $ml\,mmHg^{-1}$, for arterioles, capillaries and venules respectively. Venule capacitance is divided into the superior sagittal sinus (SSS) and inferior sagittal sinus (ISS). Vessel numbers refer to Fig. 2 for veins and to network of [18] for arteries.

scales of intracranial pressure variations due to an imbalance of CSF filtration and absorption will by several orders of magnitude longer than a cardiac cycle.

Equation (3) is solved with the forward Euler scheme and requires the computation of $\frac{dV_{cv}}{dt}$, which is approximated as

$$\frac{dV_{cv}^n}{dt} = \frac{V_{cv}^n - V_{cv}^{n-1}}{\Delta t}\,,$$

where superscript n refers to the current time step of the simulation.

The initial volume of each compartment is computed as follows:

- the volume of intracranial vascular compartments is: $V_a = 30\,ml$, $V_{al} = 16\,ml$, $V_{cap} = 20\,ml$, $V_{ven} = 70\,ml$ and $V_v = 13\,ml$, for arteries, arterioles, capillaries, venules and veins, respectively [14].

- The initialization pressures for arteries $P_a^0 = 70\,mmHg$ and for veins $P_v^0 = 5\,mmHg$ define the volumes of intracranial arteries and veins, $V_a = 3.52\,ml$ and $V_v = 20.36\,ml$.

- Then, we set $V_{al} = 16\,ml + (30\,ml - V_a)$, $V_{cap} = 20\,ml$ and $V_{ven} = 70\,ml + (13\,ml - V_v)$.

- These volumes correspond to $V_{cv}^0 = 162\,ml$, with a distribution of cerebral blood volume (CBV) between arteries-arterioles and capillaries-venules-veins over total volume of 30 % and 70 %, respectively.

- The volume of each compartment is updated at each time step by the mass conservation principle.

The computed intracranial pressure will act on intracranial one-dimensional vessels, as well as on lumped-parameter models, as a prescribed external pressure $p_e(x,t)$ in (2).

2.3 Starling resistor

The pressure difference that governs cerebral blood flow (CBF) in physiological conditions is the Cerebral Perfusion Pressure (CPP), defined as the difference between arterial and intracranial pressure [10, 15, 21]. This behaviour of CBF, where the downstream pressure is the intracranial pressure and not the central venous pressure, was the reason for the medical community to consider CBF as a flow phenomenon governed by a *Starling resistor* [12].

The Starling resistor is an experimental device in which a collapsible tube is connected to two rigid tubes at its extremities and located in a chamber of fixed volume with variable ambient pressure [4]. One can change inlet, outlet and chamber pressure (often called external pressure) and observe the resulting flow patterns. The collapsible nature of the tube produces peculiar effects, such as *flow limitation*. In practice, there is a range of pressure values for which the flow rate through the tube becomes practically independent of the downstream pressure and the dominant pressure difference is given by the upstream and external pressures. This happens when the external pressure is much higher than the outlet pressure. For a thorough analysis of the mathematical background of flow limitation the reader is referred to [22], for example.

There is undeniable experimental evidence suggesting that for physiological conditions the brain as a whole behaves as a Starling resistor [9, 15, 21]. Intracranial veins are flexible thin-walled tubes surrounded by the brain parenchyma or CSF, depending on their location, that drain into the various dural sinuses (superior sagittal, inferior sagittal, straight and transverse sinuses). Dural sinuses are located in the dura matter and are therefore considerably more rigid than cerebral veins. Moreover, there is evidence of drastic variations of the morphology and mechanical properties of cerebral veins in the vicinity of their confluence with the dural sinuses [29, 5, 6, 30, 3]. These considerations have led to the hypothesis that the terminal portion of cerebral veins acts as a Starling resistor [10, 15, 1]. These observations are supported by pressure measurements in animals [10, 15] that indicate that the relation

$$p_a \geq p_{cv} \geq p_{ic} \geq p_{ds} \tag{5}$$

holds for a wide range of p_{ic} values. Here p_a, p_{cv} and p_{ds} are arterial, cerebral venous and dural sinuses pressures, respectively.

As a first attempt to model this phenomenon, we introduce a Starling resistor (SR) in the terminal portion of cerebral veins of our venous network. We follow [19], who made use of this concept to model the zero-flow pressure in capillary beds. Flow across the SR element is

$$q_{SR} = \begin{cases} \dfrac{p_{up} - p_{ic}}{R_{SR}}\,, & \text{if } p_{down} \leq p_{ic}\,, \\ \dfrac{p_{up} - p_{down}}{R_{SR}}\,, & \text{if } p_{down} > p_{ic}\,, \end{cases} \tag{6}$$

where p_{up} and p_{down} are pressures upstream and downstream of the SR element with respect to flow towards the heart. The resistance to flow in the SR element is taken as

$$R_{SR} = \begin{cases} R^0_{SR}\,, & \text{if } p_{up} \geq p_{ic}\,, \\ \infty\,, & \text{if } p_{up} < p_{ic}\,, \end{cases} \tag{7}$$

where R^0_{SR} is a reference resistance; considering that flow rate in individual cerebral veins is always below $1\,ml\,s^{-1}$, we choose $R^0_{SR} = 1\,mmHg\,ml^{-1}\,s$. By doing so, we create a moderate pressure drop across the SR element, when open. Note that if the external pressure p_{ic} is higher than the venous pressure p_{up}, the SR element collapses completely and does not allow for flow. Moreover, if the downstream pressure p_{down} is lower than the external pressure p_{ic}, flow across the SR element is limited to that given by the pressure difference between the cerebral vein p_{up} and the external pressure p_{ic}. SR elements are placed in the vicinity of where cerebral veins connect to dural sinuses. Table 3 shows the pairs of vessels between which an SR element has been placed.

No.	Left vessel index	Right vessel index
1	158	261
2	159	262
3	161	263
4	162	264
5	237	265
6	238	266
7	239	267
8	249	268
9	245	269
10	260	270
11	271	106
12	150	272
13	151	273

Table 3: Location of Starling resistor elements in the venous network shown in Figure 2.

2.4 Venous valves

One distinct aspect of veins is the presence of valves. In particular, concerning extracranial veins, it is known that about 90 % of the population has valves [28]. Therefore, a model aimed at simulating the complete haemodynamics must account for this fact. Here we adopt a valve model that is different from that of [18]. Venous valves are located between two one-dimensional vessels and govern flow across this interface. Here we adopt the model proposed in [20], where time variation of flow rate q_v across the valve, is given as

$$\frac{dq_v}{dt} = \frac{1}{L}\left(p_{up} - p_{down} - Bq_v|q_v|\right)\,, \tag{8}$$

where p_{up} and p_{down} are upstream and downstream pressures, with respect to valve flow direction. L is a blood inertance parameter and B is a resistive parameter due to flow separation and are computed as

$$L = \frac{\rho l_{eff}(t)}{A_{eff}(t)}\,, \quad B = \frac{\rho}{2A^2_{eff}(t)}\,. \tag{9}$$

$A_{eff}(t)$ is the effective area of the valve, while $l_{eff}(t)$ is taken to be the diameter of $A_{eff}(t)$. The effective area varies according to the valve state $\zeta(t) \in (0, 1)$ in

the following manner

$$A_{eff}(t) = (A_{eff,max} - A_{eff,min}))\,\zeta(t) + A_{eff,min}\,. \tag{10}$$

In order to allow the modelling of healthy and pathological situations, $A_{eff,min}$ and $A_{eff,max}$ are defined as

$$A_{eff,min} = M_{rg}A_{ann}\,, \quad A_{eff,max} = M_{st}A_{ann}\,. \tag{11}$$

A_{ann} is called annulus area and is normally taken as the average of the reference area of the two vessels connected to the valve. As specified in [20], setting $M_{rg} = 0$ and $M_{st} = 1$ corresponds to a healthy valve, while $M_{rg} > 0$ corresponds to an incompetent valve, and $M_{st} < 1$ represents a stenotic valve. The valve state $\zeta(t)$ is governed by

$$\frac{d\zeta}{dt} = \begin{cases} (1-\zeta)K_{vo}\,(\Delta p - \Delta p_{vo})\,, & \text{if } \Delta p = p_{up} - p_{down} > \Delta p_{vo}\,, \\ \zeta K_{vc}\,(\Delta p - \Delta p_{vc})\,, & \text{if } \Delta p < \Delta p_{vc}\,, \end{cases} \tag{12}$$

where Δp_{vo} and Δp_{vc} are opening and closure threshold pressures, here taken to be $\Delta p_{vo} = \Delta p_{vc} = 0\,mmHg$ and K_{vo} and K_{vc} are opening and closure rates taken to be $K_{vo} = K_{vc} = 1.0\,Pa^{-1}\,s^{-1}$.

3 Results

Here we first describe the basic setting of the simulations and then present computational results, focusing our attention on head and neck veins. We conclude by performing a set of simulations in which different components of the model are switched on and off in order to assess their influence on the shaping of cerebral venous flow waveforms.

3.1 Model setting

One-dimensional vessels are discretesed into computational cells of mesh size $\Delta x = 1\,cm$, imposing that a single vessel should contain at least 3 computational cells. Equations (1) and (2) are solved numerically by first reformulating them [25] and then deploying a modern numerical method [17]. For background on modern numerical methods for hyperbolic equations see [24].

The friction loss term f is taken as $f = 8\,\pi\,\mu u/\rho$, with $\mu = 0.0045\,Pa\,s$ and $\rho = 1060\,kg/m^3$. At time $t = 0$, $u(x,0) = 0\,m/s$ is imposed in the entire network and pressure $p(x,0)$ in each model compartment is set as specified in Table 4. A periodic solution is obtained after 15-16 cardiac cycles. Results shown in the following sections are for the time interval $18\,s \le t \le 19\,s$.

3.2 Computational results *versus* MRI measurements

Fig. 4 shows a comparison of computed results against MRI measurements of cardiac-cyle averaged flow rates, for a selected set of cerebral vessels. The agreement between computed and measured quantities is satisfactory. Flow distribution amongst cerebral vessels is reproduced well, though these quantities do not contain information on waveforms. Such description is represented in Figs. 5 and 6, which show a comparison of flow rate waves obtained by computation and MRI measurements, together with computed pressure waves. As for time-averaged quantities, the agreement is satisfactory.

Compartment	$p(x,0)\,[mmHg]$
Arteries	70.0
Veins	5
Heart chambers & pulmonary compartments	10.0
Arterioles	45.0
Capillaries	25.0
Venules	10.0
Intracranial pressure	9.0

Table 4: Inital pressure values for all compartments of the closed-loop model.

3.3 Starling resistor and intracranial pressure effects on cerebral venous haemodynamics

Fig. 7 shows the computed pressure in the superior sagittal sinus and in a cerebral vein, together with the intracranial pressure for four model settings depicted in Figs. 7a to 7d. In Fig. 7a we observe the effect of including both, the intracranial pressure and the SR elements. Pressure in cerebral veins is always higher than intracranial pressure, while pressure in the superior sagittal sinus is governed by downstream conditions. If the SR elements are not considered, as shown in Fig. 7b, cerebral veins and the superior sagittal sinus are directly connected, resulting in lower cerebral venous pressures. Another consequence of not considering SR elements is the lower intracranial pressure values, see Fig. 7b, compared to those when SR elements are present, see Fig. 7a. These lower values for intracranial pressure are a consequence of a reduction in the volume of cerebral veins. Results excluding the time variation of intracranial pressure over time are analogous to those previously discussed, see Figs. 7c and 7d.

Another interesting effect of SR elements on cerebral venous haemodynamics is the reduction of pulsatility of velocity in cerebral vessels, as shown in Fig. 8. The reduced pulsatility of intracranial pressure as compared to the pulsatility of pressure in the dural sinuses greatly reduces the pulsatility of flow in cerebral veins and, as a consequence, in dural sinuses. This pulsatility reduction improves the agreement between computational results and MRI-derived flow rate waveforms, as shown in Fig. 9.

4 Discussion

Here we discuss our computed results concerning flow distribution, intracranial pressure and cerebral venous flow waveforms.

The flow distribution between superior sagittal and straight sinus in this model is mainly determined by the configuration of the microcirculation network and affluent cerebral veins. These networks were constructed taking into account the rather constant ratio of flow distribution between superior and straight sinuses [23]. The same inter-subject homogeneity observed for flow distributions ratios between straight and superior sagittal sinuses is not found between left and right transverse sinuses and, consequently, between left and right internal jugular veins [23]. The agreement of flow distribution in these vessels between computational results and MRI-derived data, as shown in Fig. 4, is a result of the patient-specific characterization performed for major head and neck veins,

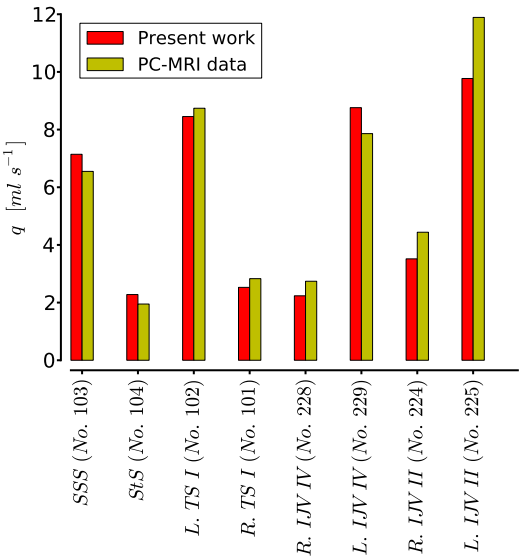

Figure 4: Cardiac-cycle averaged flow rate in head and neck veins: computational results *versus* MRI flow quantification data. SSS: Superior sagittal Sinus; StS: Straight Sinus; TS: Transverse Sinus; IJV: Internal Jugular Vein. Vessel numbers refer to Figure 2 and Table 1.

as shown in [18].

The shape of the intracranial pressure wave is defined by the interaction of variations in CBV and CSF exchange between the cranial and spinal subarachnoid spaces. Based on 65 short-term pressure recordings on patients with a variety of intracranial disorders, Avezaat *et al.* [2] showed that mean pulsatile change in CBV is 1.6 ml (0.36 ml - 4.38 ml). In our model this value is around 1 ml. Moreover, cerebral arterial plus arteriolar blood volume is 30% of total CBV, while venous plus capillary fraction is around 70%, in agreement with measurements reported in [8]. This distribution pattern was assigned as initial condition, see section 2.2, and is maintained throughout the cardiac cycle, as shown in Fig. 10. The role played by each vascular compartment in shaping intracranial pressure can be better understood by considering Fig. 11, which shows the time variation of blood volume V minus the average blood volume V_{av} occupied by each compartment. The leading compartment in terms of volume changes is the one representing distal arteries and arterioles. On the other hand, veins seem to play a rather passive role, being compressed by high intracranial pressure and expanding during the diastolic phase.

The shape of flow rate waveforms in dural sinuses is less pulsatile than venous flow in neck veins [23]. This observation is also found in the MRI measurements reported in the present work and confirmed by our computational results.

Some authors claim that the pulsatility of cerebral venous flow is due to the compression of venous vasculature by intracranial pressure and use this concept to reproduce the jugular venous flow waveforms [11]. The results presented in this work suggest that this phenomenon influences cerebral venous flow only marginally and could by no means be the explanation of venous flow waveforms at the level of internal jugular veins. In fact, volume changes in venules and

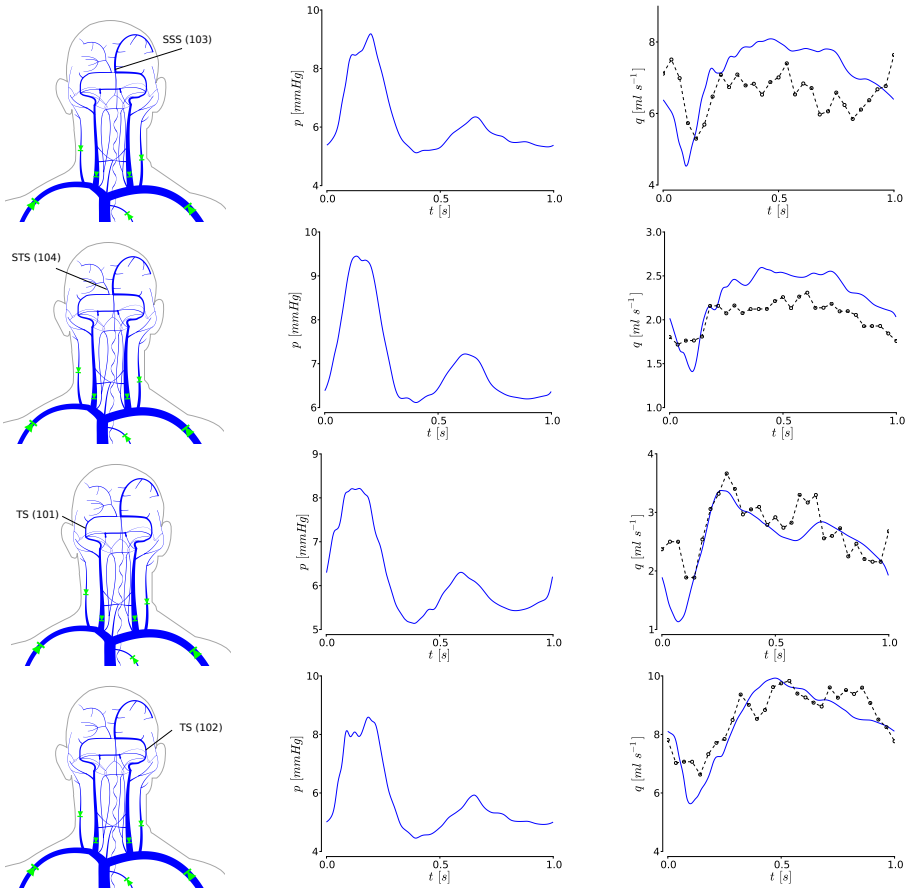

Figure 5: Computed pressure and flow rate in dural sinuses. PC-MRI flow quantification data is shown with symbols and dashed lines.

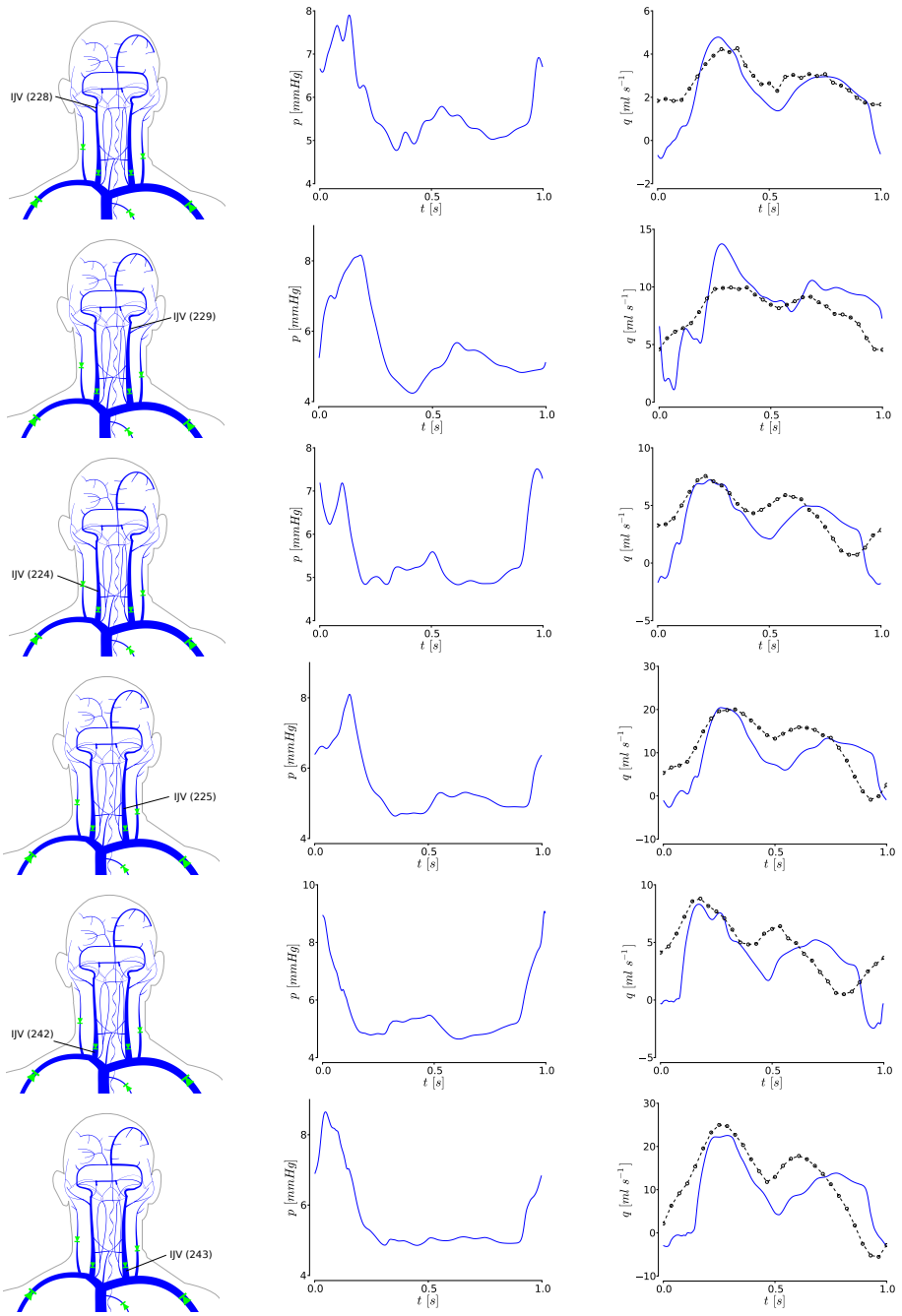

Figure 6: Computed pressure and flow rate in internal jugular veins. PC-MRI flow quantification data is shown with symbols and dashed lines.

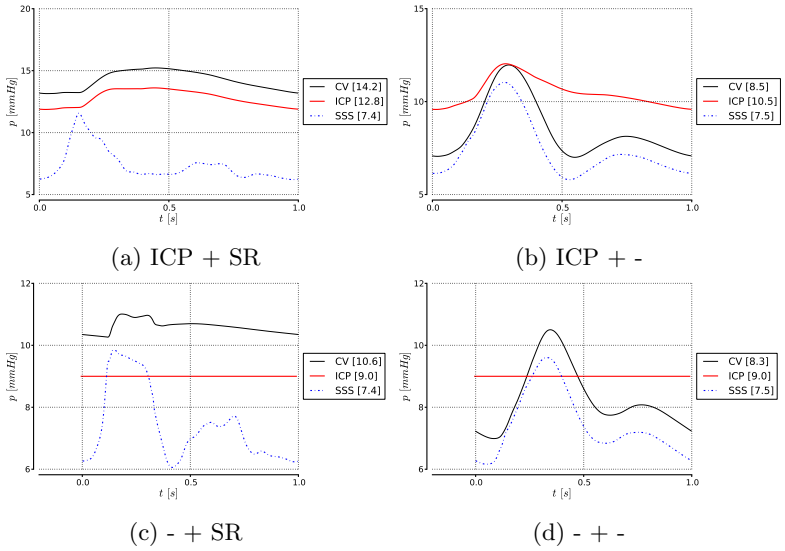

(a) ICP + SR (b) ICP + -

(c) - + SR (d) - + -

Figure 7: Effect of a Starling resistor element and intracranial pressure on computed pressures. Results obtained using: (a) variable intracranial pressure and SR elements; (b) variable intracranial pressure and no SR elements; (c) constant intracranial pressure and SR elements; (d) constant intracranial pressure and no SR elements. CV: cerebral vein (No. 158); ICP: intracranial pressure; SSS: superior sagittal sinus (No. 165).

veins over the cardiac cycle are rather modest, as shown in Fig. 11.

The model component that mainly influences the shape of cerebral venous flow rate waveforms is the presence of Starling resistor elements. These elements guarantee a pressure difference between cerebral veins and dural sinuses that is favourable to flow towards the heart over the entire cardiac cycle. Removing the SR elements from the network results in highly pulsatile flow in all dural sinuses, as shown in Fig. 9.

5 Concluding remarks

We have extended the closed-loop model for the cardiovascular system with emphasis in the cerebral venous system presented in [18], in order to account for the effect of intracranial pressure and Starling resistor elements on cerebral venous haemodynamics. Computational results have been compared to MRI-derived flow measurements, observing overall agreement. Major determinants of cerebral venous flow waveforms have been studied and discussed. The present model is a computational tool suitable for the study of pathologies related to extracranial venous anomalies and their interaction with intracranial haemodynamics, which are the subject of future investigations.

It is fair to mention that the proposed model has some limitations. The intracranial pressure lumped-parameter model used here does not admit spatial variability. Consequently, pressure changes affect all vascular components instantaneously and in the same manner. In order to gain a deeper understanding on the effect of blood flow on CSF dynamics, the model should include a more

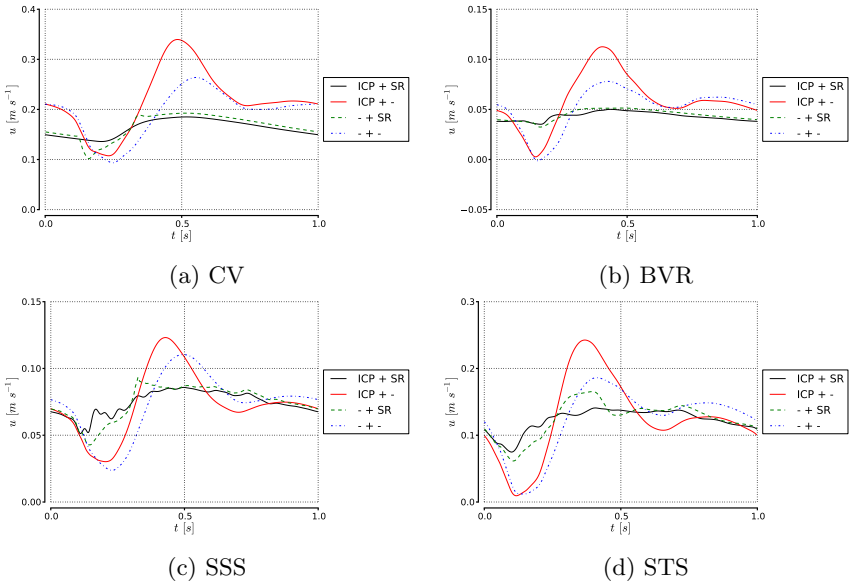

(a) CV (b) BVR

(c) SSS (d) STS

Figure 8: Effect of a Starling resistor element and intracranial pressure on computed velocity in cerebral venous vessels. CV: cerebral vein (No. 158); BVR: basal vein of Rosenthal (No. 247); SSS: superior sagittal sinus (No. 165); STS: straight sinus (No. 104).

sophisticated description for intracranial pressure. Such model should be able to account for the space- and time-dependent CSF dynamics.

Conflict of interest statement

None.

Acknowledgements

The authors warmly thank Prof. E. M. Haacke (MR Research Facility, Wayne State University, Detroit, USA) for providing MRI data used in this work. This work has been partially funded by CARITRO (*Fondazione Cassa di Risparmio di Trento e Rovereto*, Italy), project No. 2011.0214.

References

[1] C. Anile, P. De Bonis, A. Di Chirico, A. Ficola, A. Mangiola, and G. Petrella. Cerebral blood flow autoregulation during intracranial hypertension: a simple, purely hydraulic mechanism. *Childs Nervous System*, 25:325–335, 2009.

[2] C. J. Avezaat and J.M. Eijndhoven. The role of the pulsatile pressure variations in intracranial pressure monitoring. *Neurosurgical Review*, 9(1-2):113–120, 1986.

[3] J. Chen, X. Wang, L. Luan, B. Chao, B. Pang, H. Song, and Q. Pang. Biological characteristics of the cerebral venous system and its hemodynamic response to intracranial hypertension. *Chinese Medical Journal*, 125:1303–1309, 2012.

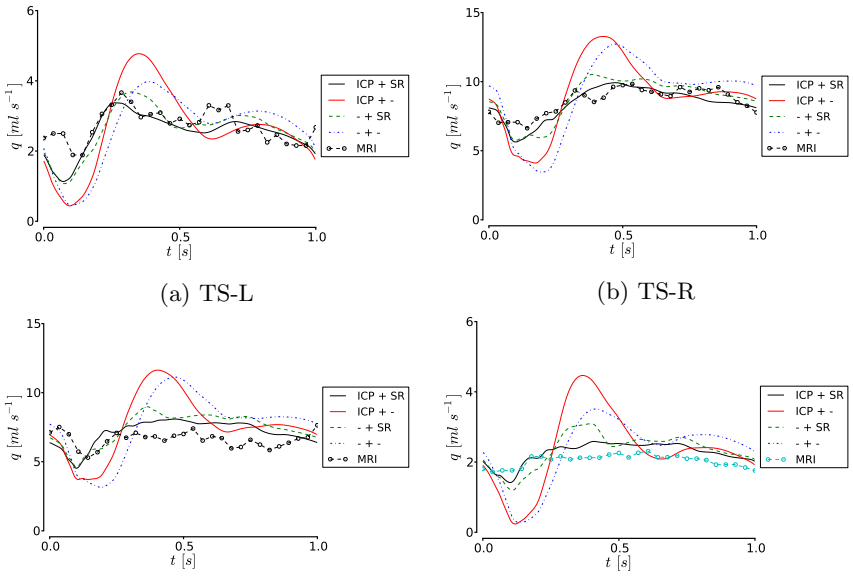

(a) TS-L (b) TS-R

(c) SSS (d) STS

Figure 9: Effect of a Starling resistor element and intracranial pressure on computed flow rate in dural sinuses. TS-R: right transverse sinus (No. 101); TS-L: left transverse sinus (No. 102); SSS: superior sagittal sinus (No. 103); STS: straight sinus (No. 104).

[4] W. A. Conrad. Pressure-flow relationships in collapsible tubes. *IEEE Transactions on Biomedical Engineering*, 16(4):284–295, 1969.

[5] A. Dagain, J.R. Vignes, R. Dulou, G. Dutertre, J.M. Delmas, J. Guerin, and D. Liguoro. Junction between the great cerebral vein and the straight sinus: An anatomical, immunohistochemical, and ultrastructural study on 25 human brain cadaveric dissections. *Clinical Anatomy*, 21(5):389–397, 2008.

[6] A. Dagain, R. Vignes, R. Dulou, J. Delmas, T. Riem, J. Guerin, and D. Liguoro. Study of the junction between the cortical bridging veins and basal cranial venous sinus. *Neurochirurgie*, 55:19–24, 2009.

[7] J. Ekstedt. CSF hydrodynamic studies in man. 2. Normal hydrodynamic variables related to CSF pressure and flow. *Journal of Neurology, Neurosurgery & Psychiatry*, 41(4):345–353, 1978.

[8] H. Ito, I. Kanno, H. Iida, J. Hatazawa, E. Shimosegawa, H. Tamura, and T. Okudera. Arterial fraction of cerebral blood volume in humans measured by positron emission tomography. *Annals of Nuclear Medicine*, 15:111–116, 2001.

[9] I. H. Johnston, J. O. Rowan, A. M. Harper, and W. B. Jennett. Raised intracranial pressure and cerebral blood flow. III. Venous outflow tract pressures and vascular resistances in experimental intracranial hypertension. *Journal of Neurology, Neurosurgery & Psychiatry*, 37:392–402, 1974.

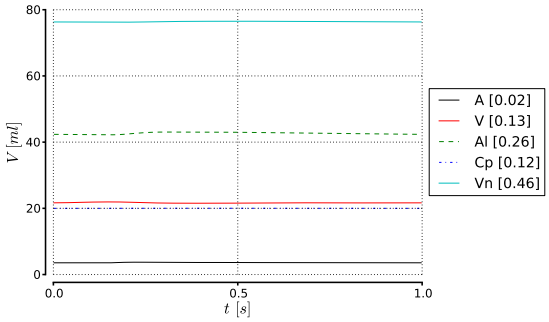

Figure 10: Cerebral blood volumes over a cardiac cycle for arteries (A), veins (V), arterioles and distal arteries (Al), capillaries (Cp) and venules (Vn). Values between square brackets represent the average fraction occupied by each compartment with respect to total cerebral blood volume.

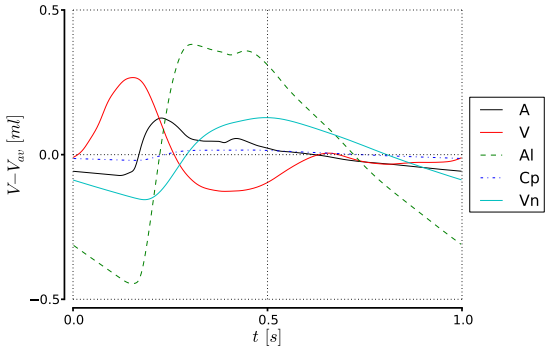

Figure 11: Variation in time of $V - V_{av}$, where V is the volume of a compartment and V_{av} is the average volume over the cardiac cycle of different compartments. Five compartments were considered, namely: A arteries; V veins; Al distal arteries and arterioles; Cp capillaries; Vn venules.

[10] I. H. Johnston, J. O. Rowan, A. M. Harper, and W. B. Jennett. Raised intracranial pressure and cerebral blood flow. IV. Intracranial pressure gradients and regional cerebral blood flow. *Journal of Neurology, Neurosurgery & Psychiatry*, 37:392–402, 1974.

[11] J. Kim, N. A. Thacker, P. A. Bromiley, and A. Jackson. Prediction of the Jugular Venous Waveform Using a Model of CSF Dynamics. *American Journal of Neuroradiology*, 28:983–989, 2007.

[12] F. P. Knowlton and E. H. Starling. The influence of variations in temperature and blood pressure on the performance of the isolated mammalian heart. *Journal of Physiology*, 44:206–219, 1912.

[13] F. Y. Liang, S. Takagi, R. Himeno, and H. Liu. Biomechanical characterization of ventricular-arterial coupling during aging: A multi-scale model study. *Journal of Biomechanics*, 42:692–704, 2009.

[14] A. A. Linninger, M. Xenos, B. Sweetman, S. Ponkshe, X. Guo, and R. Penn.

A mathematical model of blood, cerebrospinal fluid and brain dynamics. *Journal of Mathematical Biology*, 59:729–759, 2009.

[15] J. M. Luce, J. S. Huseby, W. Kirk, and J. Butler. A Starling resistor regulates cerebral venous outflow in dogs. *Journal of Applied Physiology*, 53:1496–1503, 1982.

[16] C. Magnano, C. Schirda, B. Weinstock-Guttman, D. S. Wack, E. Lindzen, D. Hojnacki, N. Bergsland, C. Kennedy, P. Belov, M. G. Dwyer, G. U. Poloni, C. Beggs, and R. Zivadinov. Cine Cerebrospinal Fluid Imaging in Multiple Sclerosis. *Journal of Magnetic Resonance Imaging*, 36:825–834, 2012.

[17] L. O. Müller and E. F. Toro. Well-balanced high-order solver for blood flow in networks of vessels with variable properties. *International Journal for Numerical Methods in Biomedical Engineering*, 29:1388–1411, 2013.

[18] L. O. Müller and E. F. Toro. A global multiscale mathematical model for the human circulation with emphasis on the venous system. *International Journal for Numerical Methods in Biomedical Engineering*, pages n/a–n/a, 2014. In Press.

[19] J. P. Mynard. *Computer modelling and wave intensity analysis of perinatal cardiovascular function and dysfunction*. PhD thesis, Department of Paedriatics, The University of Melbourne, 2011.

[20] J. P. Mynard, M. R. Davidson, D. J. Penny, and J. J. Smolich. A simple, versatile valve model for use in lumped parameter and one-dimensional cardiovascular models. *International Journal for Numerical Methods in Biomedical Engineering*, 28(6-7):626–641, 2012.

[21] S. Rossitti. Pathophysiology of increased cerebrospinal fluid pressure associated to brain arteriovenous malformations: The hydraulic hypothesis. *Surgical Neurology International*, 4(1):42, 2013.

[22] A. H. Shapiro. Steady flow in collapsible tubes. *Journal of Biomechanical Engineering*, 99:126–147, 1977.

[23] S. Stoquart-ElSankari, P. Lehmann, A. Villette, M. Czosnyka, M. Meyer, H. Deramond, and O. Baledent. A phase-contrast MRI study of physiologic cerebral venous flow. *Journal of Cerebral Blood Flow & Metabolism*, 29:1208–1215, 2009.

[24] E. F. Toro. *Riemann Solvers and Numerical Methods for Fluid Dynamics: A Practical Introduction*. Springer-Verlag, Berlin Heidelberg, third edition, 2009. ISBN 978-3-540-25202-3.

[25] E. F. Toro and A. Siviglia. Flow in collapsible tubes with discontinuous mechanical properties: mathematical model and exact solutions. *Communications in Computational Physics*, 13(2):361–385, 2013.

[26] M. Ursino. A mathematical study of human intracranial hydrodynamics part 1. The cerebrospinal fluid pulse pressure. *Annals of Biomedical Engineering*, 16(4):379–401, 1988.

[27] M. Ursino and C. A. Lodi. A simple mathematical model of the interaction between intracranial pressure and cerebral hemodynamics. *Journal of Applied Physiology*, 82:1256–1269, 1997.

[28] D. Valecchi, D. Bacci, M. Gulisano, E. Sgambati, M. Sibilio, M. Lipoma, and C. Macchi. Internal jugular vein valves: an assessment of prevalence, morphology and competence by colo doppler echography in 240 healthy subjects. *Basic and Applied Anatomy*, 115:185–189, 2010.

[29] J. Vignes, A. Dagain, J. Guerin, and D. Liguoro. A hypothesis of cerebral venous system regulation based on a study of the junction between the cortical bridging veins and the superior sagittal sinus. *Journal of Neurosurgery*, 107:1205–1210, 2007.

[30] Y. Yu, J. Chen, Z. Si, G. Zhao, S. Xu, G. Wang, F. Ding, L. Luan, L. Wu, and Q. Pang. The Hemodynamic Response of the Cerebral Bridging Veins to Changes in ICP. *Neurocritical Care*, 12(1):117–123, 2010.

[31] P. Zamboni, R. Galeotti, E. Menegatti, A. M. Malagoni, G. Tacconi, S. Dall'Ara, I. Bartolomei, and F. Salvi. Chronic cerebrospinal venous insufficiency in patients with multiple sclerosis. *Journal of Neurology, Neurosurgery and Psychiatry*, 80:392–399, 2009.

[32] R. Zivadinov, C. Magnano, R. Galeotti, C. Schirda, E. Menegatti, B. Weinstock-Guttman, K. Marr, I. Bartolomei, J. Hagemeier, A. Malagoni, D. Hojnacki, K. Kennedy, E. Carl, C. Beggs, F. Salvi, and P. Zamboni. Changes of cine cerebrospinal fluid dynamics in patients with multiple sclerosis treated with percutaneous transluminal angioplasty: A case-control study. *Journal of Vascular and Interventional Radiology*, 24(6):829–838, 2013.